CRYSTAL GROWTH & DESIGN

pubs.acs.org/crystal

Article

Synthesis and Hydrolysis of Brushite (DCPD): The Role of Ionic Substitution

Elisa Boanini,* Francesca Silingardi, Massimo Gazzano, and Adriana Bigi

Cite This: *Cryst. Growth Des.* 2021, 21, 1689−1697

Read Online

ACCESS | Metrics & More | Article Recommendations | Supporting Information

ABSTRACT: Brushite (dicalcium phosphate dihydrate, DCPD) is considered one of the possible precursors of the apatitic phase that constitutes the mineral component of bones, and it is often utilized in the preparation of biomaterials for hard tissue repair. In this work, we investigated the influence of ionic substitution on the synthesis, structure, and morphology of this calcium phosphate, as well as on its hydrolysis process. The results of structural refinements indicate that the range of possible substitution can reach values up to about 38 atom % for the big Sr ion, whereas it is quite limited for Zn, Co, and Mn. In particular, DCPD cannot be obtained as a single phase in the presence of zinc ions in solution. The kind and amount of substituent ions significantly influence the morphology of DCPD, promoting aggregation and crystal shape modifications, as well as its hydrolysis in solution. The results provide useful information for the understanding of the mineralization processes and for the design of new biomaterials.

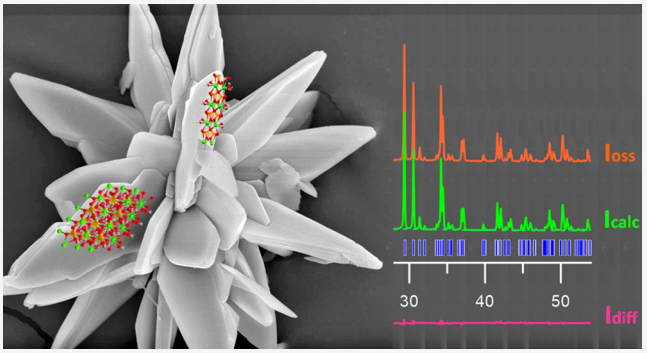

INTRODUCTION

Dicalcium phosphate dihydrate, $CaHPO_4{\cdot}2H_2O$ (DCPD), is one of the orthophosphates that find useful applications in the preparation of biomaterials for hard tissue repair. DCPD, also known by the mineral name of brushite, crystallizes in the monoclinic Ia space group. Its structure consists of parallel Ca layers with HPO_4 groups located between metal ions.[1,2] The water molecules are situated among the chains,[2] acting as spacers between calcium phosphate layers arranged parallel to each other in the *a*,*c* plane (020), as displayed in Figure 1. The two structural water molecules can be removed by heat treatment at about 190 °C, which yields transformation into anhydrous calcium phosphate, $CaHPO_4$ (DCPA).[3]

DCPD is considered one of the possible precursors of biological apatites, together with amorphous calcium phosphate (ACP) and octacalcium phosphate ($Ca_8H_2(PO_4)_6{\cdot}5H_2O$, OCP).[4−6] In particular, biological apatites have been suggested to form through a disordered DCPD and its successive transformation into hydroxyapatite.[7] However, brushite has not been found in physiological calcifications,[8] whereas it has been detected in several pathological calcifications, including dental calculi, crystalluria, and urinary stones, as well as calcified aortic valves.[9−12] On the other hand, the presence of DCPD has been demonstrated at the initial stage of in vitro osteoblast mineralization.[13]

Recently, the phase transformation of DCPD to HA has been described as a multistage process that also involves amorphous calcium phosphate.[14] In fact, DCPD formation occurs in acidic solutions at pH values between 2 and 6.[15] In aqueous solution, it undergoes hydrolysis thermodynamically more stable phases, OCP and HA.[3,16,17] This is the main reason for the widespread employment of DCPD in the composition of calcium phosphate bone cements.[18−20]

The properties of calcium phosphates can be modulated through their functionalization with ions, molecules, macromolecules, growth factors, and drugs.[21] In particular, functionalization with biologically relevant ions can provide useful information for a deeper knowledge of the biomineralization processes, as well as to tailor the properties of the inorganic phase and synthesize biomaterials with improved biological performance.[22] Ionic substitution into HA has been widely explored in the literature.[22−28] At variance, the number of publications on the interaction between foreign ions and DCPD is quite limited,[29] although the presence of foreign ions is also relevant in DCPD pathological calcifications.[30] Moreover, most of the studies are about bone cements, which are usually composed of more than one crystalline phase, preventing a clear indication of ionic incorporation into the DCPD structure.[31,32] Again, the few available publications on brushite synthesized in the presence of foreign ions generally

Received: November 18, 2020
Revised: January 28, 2021
Published: February 17, 2021

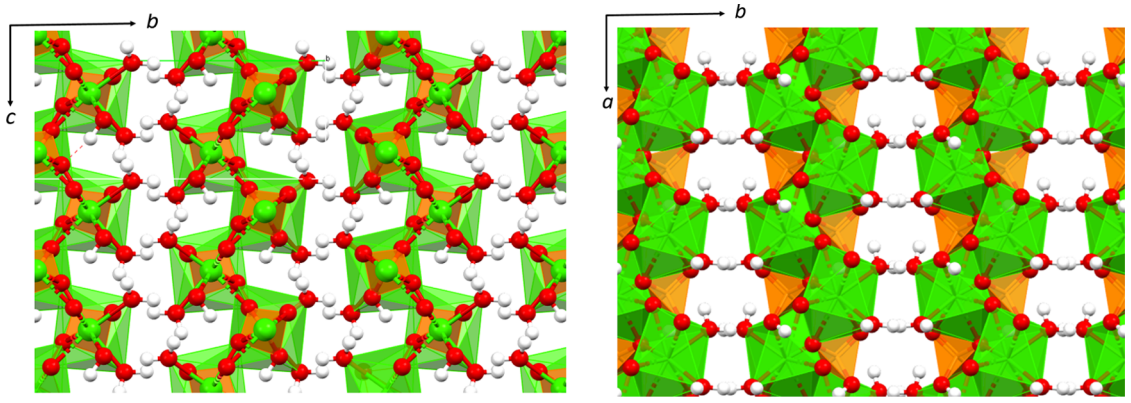

Figure 1. Structure of DCPD: view down the *a*-axis (left) or *c*-axis (right). Ca polyhedra and phosphate tetrahedra are shown in green and orange colors, respectively; oxygen and hydrogen atoms are in red and white, respectively.

do not investigate cell parameters and therefore do not provide useful information to define if the ions are regularly substituted and to what extent.[33,34] Only a recent work reported the lattice parameters of DCPD synthesized in the presence of different ions and concluded that ionic incorporation, if any, amounted to just a few atom % before the precipitation of secondary phases.[35]

Herein, we report the results of a study aimed to investigate the effects of modifications induced by ionic substitution on the chemistry, structure, and morphology of DCPD. In particular, we determined the possible substitutional range of Sr, Zn, Mn, and Co, as well as their influence on the stability of DCPD.

All of the bivalent cations examined in this study are biologically relevant. In particular, they are included as trace elements in the composition of bones.[22] As other metal ions, cobalt can induce cell oxidative stress and stimulate angiogenesis and osteogenesis.[36] Co-substituted HA was reported to accelerate new bone formation in artificially created osteoporotic defects.[37] Manganese plays a role in bone metabolism, and manganese-doped calcium phosphates have been shown to promote osteoblast proliferation and differentiation.[38] Moreover, Mn deficiency was demonstrated to increase bone abnormalities, including reduction of bone thickness and length.[39] Zinc can stimulate osteoblast activity[40] and displays antibacterial properties.[41] This ion plays an important role in the normal growth of the skeletal system, and its deficiency causes a decrease of bone density.[42] Finally, strontium is known to promote bone formation and counteract abnormally high bone resorption.[43] It is present in significant amounts in bone, especially at regions of high metabolic turnover,[44] whereas its localization has been reported not to vary between physiological and pathological apatites.[45]

The products of the syntheses of DCPD in the presence of increasing concentrations of Co^{2+}, Mn^{2+}, Zn^{2+}, and Sr^{2+}, as well the samples obtained after their hydrolysis, were characterized by X-ray diffraction, infrared absorption spectroscopy, and scanning electron microscopy.

EXPERIMENTAL SECTION

Preparation of DCPD crystals was carried out by direct synthesis in solution. A phosphate solution (150 mL) containing $Na_2HPO_4 \cdot 12H_2O$ (0.033 M) and $NaH_2PO_4 \cdot H_2O$ (0.033 M) was heated at 37 °C, and the pH was adjusted to 5 adding glacial CH_3COOH; 50 mL of a $Ca(CH_3COO)_2 \cdot H_2O$ (0.2 M) solution was added dropwise (2 mL/min) to the phosphate solution under stirring (120 rpm). After the addition, the solution was stirred for another 10 min, filtered, washed with distilled water, and dried overnight at 37 °C. Samples containing bivalent metals (M = Sr, Mn, Co, Zn) were obtained following the same procedure, but partially replacing $Ca(CH_3COO)_2 \cdot H_2O$ with $Sr(CH_3COO)_2 \cdot 1/2H_2O$ or $Mn(CH_3COO)_2 \cdot 4H_2O$ or $Co(CH_3COO)_2 \cdot 4H_2O$ or $Zn(CH_3COO)_2 \cdot 2H_2O$. All reagents were of analytical grade (Carlo Erba Reagents, Milan, Italy). Starting solutions were prepared with different $[M^{2+}/(Ca^{2+} + M^{2+})] \cdot 100$ ratios, in the range from 0 to 100, always keeping the total cation concentration of 0.2 M. In the following, the solid products synthesized in the presence of *x* atom % of M are labeled Mx.

Hydrolysis of DCPD and ion-substituted DCPD was carried out in physiological solution (NaCl 0.9%) at 37 or 60 °C. For each sample, 100 mg of powder was incubated in 25 mL of solution under stirring. The hydrolysis reaction was monitored over time, up to 7 days. After incubation, each sample was centrifuged for 10 min at 10 000 rpm and then dried at 37 °C.

Characterization. X-ray diffraction (XRD) scans were carried out with a PANalytical X'Pert PRO diffractometer in the Bragg−Brentano geometry. It was equipped with a Cu K source (λ = 1.5418 Å, 40 mA, 40 kV), and data were collected with a fast X'Celerator detector. All patterns were collected in the 2θ range of 3−60° for 80 s for each 0.1° step, and in addition further collections were performed as input for the Rietveld procedure in the range 8−80° for 100 s for each 0.033° step. The HighScore Plus program was used for phase identification, quantitative determination of the different phases, and structural refinements (HighScore Plus software version 4.9, year 2020, by PANalytical B.V., Almelo, The Netherlands).

Scattering factors of Ca^{2+}, Me^{2+}, P^{5+}, and O^{2-} ions were employed. At the beginning, the free parameters were scale factor, background coefficients, and 2θ shift. In further cycles, cell axes, peak widths, their dependence on 2θ, peak shape, preferential orientation, and peak asymmetry were added as free variables. Finally, the overall thermal parameter and structural parameters (occupancy factors) were refined. Substituent ions were placed in the same position as calcium with the constraint that the total content of calcium and substituent ion must be equal to unity.

For Fourier transform infrared spectroscopy (FTIR) analysis, about 1 mg of the powdered samples was mixed with 250 mg of KBr (infrared grade) and pelletized under a pressure of 9 tons. The pellets were analyzed using a Bruker α FTIR spectrophotometer to collect 32 scans in the range 4000−400 cm^{-1} at a resolution of 4 cm^{-1}.

To perform morphological investigation and elemental analysis, a Philips XL20 scanning electron microscope operating at 22 kV was used. The samples were placed on a carbon tape on aluminum sample holders, and elemental analysis was carried out through energy-dispersive X-ray spectroscopy (EDX); afterward, samples were sputter-coated with a layer of gold for morphological examination.

https://dx.doi.org/10.1021/acs.cgd.0c01569
Cryst. Growth Des. 2021, 21, 1689−1697

RESULTS AND DISCUSSION

Synthesis and Screening of Substitution Ranges. XRD analysis was carried out on the solid products of the syntheses performed in the presence of different amounts of foreign cations. The results indicate that the range of possible substitution to calcium into the DCPD structure is quite different for different ions. The synthesis carried out in the absence of foreign ions yields DCPD as a unique crystalline phase (ICDD PDF 00-009-0077). The XRD pattern of pure DCPD (Figure 2) shows sharp peaks with a high relative intensity of 0*k*0 reflections, coherently with the platelike morphology of the crystals, characterized by wide (010) faces.

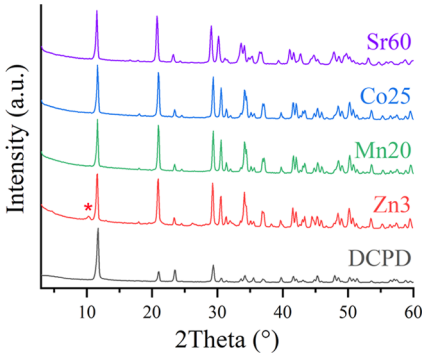

Figure 2. X-ray diffraction patterns: DCPD, Mn20, Co25, and Sr60 powders are composed of a single-crystalline phase, whereas the presence of zinc always induces the formation of parascholzite (ICDD PDF 00-035-0495) as a secondary phase. The main peak of parascholzite is indicated by an asterisk.

The results of XRD analysis demonstrate that the presence of foreign cations in solution hinders the formation of DCPD as a unique crystalline phase in different ways depending on the kind of metal and its concentration.

The products obtained in the presence of increasing Sr^{2+} concentration in solution exhibit XRD patterns consistent with the presence of DCPD as a unique crystalline phase up to Sr60 (Figure 2), whereas the pattern of Sr70 is almost devoid of diffraction reflections and is in agreement with the presence of an amorphous material (Figure S1).

In the case of Mn^{2+}, DCPD can be precipitated as a unique crystalline phase up to Mn20 (Figure 2), whereas the pattern of Mn25 also shows the presence of a secondary phase, $(Mn)_3(PO_4)_2{\cdot}7H_2O$ (ICDD PDF 00-041-0598), as well as of an amorphous phase, which becomes predominant in Mn30 (Figure S1). The range of strontium concentrations that gives DCPD without secondary phases is significantly wider than that previously obtained by Sayahi et al.,[35] and this might be ascribed to the different methods of synthesis employed in the present work.

A completely different behavior was shown by zinc ions. Even a very small amount of Zn^{2+} in solution triggers the precipitation of parascholzite, $CaZn_2(PO_4)_2{\cdot}2H_2O$ (ICDD PDF 00-035-0495), as a secondary phase (Figure 2). In agreement, the presence of a secondary phase together with DCPD was previously reported in the samples synthesized in the presence of a very small percentage of Zn in solution, which prevented a clear conclusion about Zn substitution into the DCPD structure.[35]

A secondary phase, $Co_3(PO_4)_2{\cdot}8H_2O$ (ICDD PDF 00-033-0432), can be detected in the XRD patterns of Co30 and Co40, whereas the patterns of the samples obtained at smaller Co concentrations exhibit only the peaks of DCPD (Figure S1).

Moreover, both the series of materials synthesized in the presence of Co and Mn, as well as the samples at a relatively high Sr content, show a significant reduction of the relative intensity of the 020 reflection with respect to that shown in the XRD pattern of pure DCPD.

Furthermore, different ions exerted different inhibition effects on the precipitation of DCPD, as clearly indicated by the yield of reaction, which decreases on increasing the concentration of the foreign ion down to about 40% in samples Mn20, Co25, and Sr40 (Table S1).

Structural Analysis. The ionic substitutions in the DCPD structure were investigated by structural refinements, which were carried out with the Rietveld method.[46]

Full-pattern analyses were carried out on selected samples, namely, Sr10, Sr30, Sr60, Co25, Mn20, and Zn10, as well as on unsubstituted DCPD samples for comparison. The refinements were based on the DCPD monoclinic structure, space group Ia (no. 9),[47] and reached convergence and good agreement indexes. The obtained results are summarized in Table 1. Final plots are presented in Figure 3 (sample Sr60) and Figures S2–S7.

The results unambiguously confirmed that each sample is a unique DCPD crystal phase in Co, Mn, and Sr samples, whereas sample Zn10 also contains parascholzite (15 wt %) and an amorphous material (10 wt %). Strontium-containing samples show that unit cell parameters increasingly grow as the amount of strontium in solution increases, in agreement with the partial substitution of the bigger Sr ion (ionic radius: 0.126 nm) for a Ca ion (ionic radius: 0.112 nm) into the DCPD

Table 1. Cell Parameters, Metal Content (Calculated and Analytical), and Intensity Ratio I_{020}/I_{-221} of Substituted DCPD Samples

	a (Å) ± 0.0003	b (Å) ± 0.0004	c (Å) ± 0.0002	β (°) ± 0.05	V (Å^3) ± 0.2	M/(M + Ca) Rietveld (atom %)[a]	M/(M + Ca) anal. (atom %)[b]	I_{020}/I_{-221}[c]	R_p (%)
DCPD	6.3685	15.1929	5.8179	118.53	494.5	0	0	33	8.64
Co25	6.3709	15.1973	5.8171	118.52	494.8	2	3	9	7.01
Mn20	6.3671	15.1778	5.8105	118.57	493.1	7	7	2	3.80
Sr10	6.3815	15.2124	5.8233	118.47	496.9	3	4	25	9.00
Sr30	6.4031	15.2429	5.8323	118.40	500.7	11	13	18	8.50
Sr60	6.4640	15.3485	5.8627	118.27	512.3	38	34	3	4.79
Zn10[d]	6.3661	15.1940	5.8146	118.53	494.1	5	10	2	5.26

[a]From the refinement procedure. [b]From analytical data. [c]Ratio between areas of the 020 and −221 peaks; the theoretical value with no preferred orientation is 2. [d]Sample containing a further crystal phase.

https://dx.doi.org/10.1021/acs.cgd.0c01569
Cryst. Growth Des. 2021, 21, 1689−1697

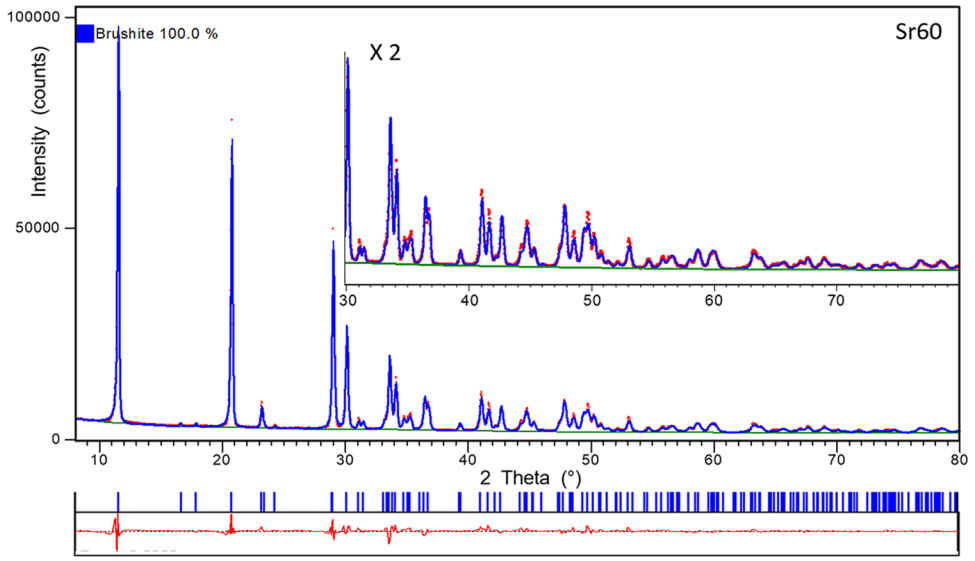

Figure 3. Comparison of the observed (red dots) and calculated (blue line) patterns of Sr60. At the bottom, vertical bars indicate peak positions of the DCPD structure; the red line indicates the $I_o - I_c$ difference plot. The inset shows a magnification (×2) of the intensity scale.

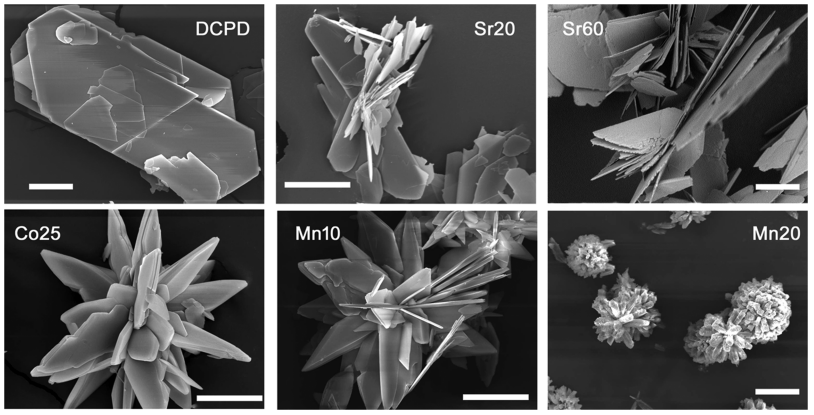

Figure 4. SEM images of DCPD, Sr20, Sr60, Co25, Mn10, and Mn20 crystals. Scale bar = 20 μm.

structure. On the other hand, the cell volume variation for the samples prepared in the presence of Co, Mn, and Zn, which have smaller ionic radii than calcium (0.90, 0.96, and 0.90 nm for Co, Mn, and Zn, respectively), is very small with respect to that of pure DCPD. This can be ascribed to the limited content of substituting cations in Co25, Mn20, and Zn10. In fact, the values of metal contents (refined to the final values reported in Table 1) indicate that the amount of calcium replacement in the solid structures is severely less than the content of foreign ions in the synthesis solution. In particular, on the basis of the refinement data, the replacement of calcium into the DCPD structure seems very limited for Co, Zn, and Mn: 2, 5, and 7 atom %, respectively. On the contrary, the substitution increases up to 38 atom % for strontium, suggesting that the DCPD crystal structure can better accommodate bigger cations than smaller ones. Although EDX results can be considered semiquantitative, data presented in Table 1 show a good agreement between the values of the metal content determined by EDX analysis and through structural refinement.

Morphology. The high preferential orientation of brushitic samples affects their XRD patterns, which display an extremely intense 020 peak. A roughly quantitative estimate of this effect can be obtained from the ratio between the relative intensities of the 020 and −221 peaks. Data reported in Table 1 show that this ratio is high in pure DCPD, as well as in strontium-substituted samples up to Sr30, whereas it strongly decreases in the Sr60 sample and in the other substituted samples.

The high preferential orientation of DCPD is a consequence of its laminar morphology; indeed, the crystals grow as big platelike crystals with sharp edges and large (010) faces (Figure 4). Although great care was taken in sample preparation, the crystals tend to lie flat on the plane of the sample holder, with a relatively high fraction of the (010) planes preferentially aligned along the specimen surface and a consequent relatively high intensity of the corresponding 0k0 XRD peaks.[48]

The presence of foreign ions displays a significant influence on the morphology of DCPD. The scanning electron microscopy images shown in Figure 4 demonstrate that strontium substitution for calcium induces aggregation of the crystals that exhibit indented edges. Aggregation of crystals increases whereas their dimensions decrease on increasing the Sr content, and therefore, at the maximum amount, Sr60 appears to be composed of spherulitic aggregates of relatively small crystals. Aggregation of crystals was also previously observed in the presence of different additives[3] and suggested that the perturbation of the DCPD structure triggered by the

https://dx.doi.org/10.1021/acs.cgd.0c01569
Cryst. Growth Des. 2021, 21, 1689−1697

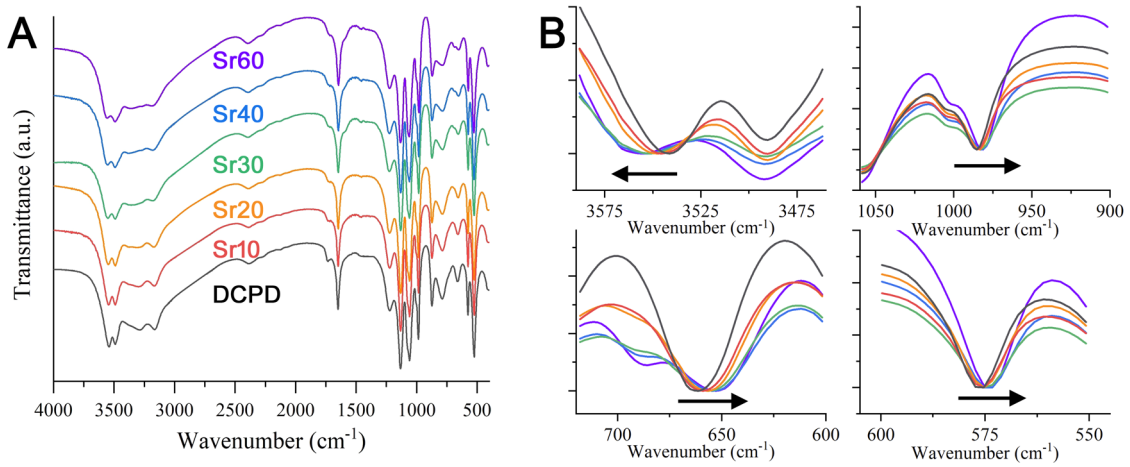

Figure 5. (A) FTIR spectra of Sr-substituted DCPD. (B) Magnifications showing the shift and widening of some relevant bands. Arrows indicate the band shift direction on increasing the Sr content.

presence of foreign agents reduced the crystal growth and promoted the interaction of crystals.

Even greater modifications are appreciable in the crystals grown in the presence of Co and Mn. Co25 contains only about 2 atom % of cobalt ions and displays aggregates of pointed crystals with a greater thickness than that characteristic of pure DCPD crystals. Similar, but definitely less thick, aggregates are detected in Mn10, whereas the aggregates present in Mn20, with a manganese content of about 7 atom %, are much smaller and composed of almost cylindrical crystals.

A significant variation in the morphology of DCPD synthesized in the presence of Co and Mn, as well as of the crystals synthesized at a relatively high Sr concentration, reduces the preferential orientation in agreement with the observed reduction of the relative intensity of the 020 XRD reflection in comparison to that of pure DCPD.

Spectroscopic Investigation. The results of attenuated total reflectance (ATR)-FTIR analysis are in agreement with those of the XRD investigation. Spectra of brushite synthesized in the presence of Sr, Co, and Mn show the characteristic absorption bands of DCPD.[49,50] However, the comparison with the spectrum of pure DCPD confirms that the presence of increasing amounts of foreign ions induces a progressive slight broadening and a shift of the absorption bands (Figures 5 and S8). This is most evident in the case of Sr, as shown in Figure 5. The bands displaying the largest shifts are the OH stretching at 3541 cm^{-1}, the PO stretching at 986 cm^{-1}, and the PO bending at 662 and 576 cm^{-1}. The position of OH stretching shifts to higher wavenumbers up to 3556 cm^{-1} in Sr60, whereas those of PO stretching and bending shift to lower frequencies, down to 980 and 653 and 573 cm^{-1}, respectively (Table S2). This behavior is similar to what was previously reported for Sr-substituted hydroxyapatites, where the shift of the phosphate bands at lower wavenumbers on increasing the Sr content was ascribed to the increasing ionic radius, which caused a decreasing anion−anion repulsion.[51]

The variation of the position of the absorption bands is much less evident for Mn-containing samples, whereas it is not considerable for Co samples, which is not surprising because of the very low amount of Co (Figures S8 and Table S2).

Hydrolysis. It is known that storing DCPD in aqueous solution triggers its transformation into thermodynamically more stable phases.[3,52] Herein, the influence of foreign ions on the process of hydrolysis was studied on samples stored in physiological solution for up to 1 week. The results in Figure 6 and Table S3 show that only 3 h of incubation in the physiological solution is sufficient for a partial conversion of pure DCPD into OCP (ICDD PDF 00-26-1056) at 37 °C and into HA (ICDD PDF 00-009-0432) at 60 °C (Figure 7). Longer immersion times lead to a complete conversion of pure DCPD into OCP and HA, confirming that the kinetics process is accelerated by the increase of the time at 60 °C.[3,17]

Functionalization with Co induces only a minor effect on the hydrolysis process, which appears to be slightly inhibited by the presence of a foreign ion.

However, Mn significantly stabilizes DCPD, as it does not convert into any other phase at 37 °C even after 1 week. After 3 h at 60 °C, Mn20 shows a partial conversion of DCPD into OCP, which becomes the only crystalline phase after 6 h. However, longer immersion times lead to a partial conversion of DCPD into β-TCP (ICDD PDF 00-009-0169), which becomes the only detectable phase after 1 week, as shown in Figure 7. This result is quite unexpected since the synthesis of β-TCP usually requires treatment at high temperatures.[53,54] Moreover, the comparison of the lattice parameters of this phase with those reported for pure β-TCP (Table S4) indicates a partial substitution of Mn for Ca in the structure of β-TCP. A similar behavior was previously observed for magnesium ions. The presence of Mg^{2+} in the aging solution of DCPD was reported to yield the mineral phase of β-TCP (whitlockite, $Ca_9Mg(HPO_4)(PO_4)_6$, ICDD PDF 00-042-0578) formed at the expense of brushite crystals, which was interpreted to proceed through a dissolution/reprecipitation process.[55]

The results of the synthesis of brushite in the presence of foreign ions demonstrate that Sr substitution for calcium into DCPD does not significantly destabilize its structure. In agreement, functionalization with strontium up to Sr40 does not alter significantly the hydrolysis process at 37 °C, whereas the conversion of Sr60 triggers the formation of an unknown crystalline phase (Figure 7). This unknown phase does not appear when the hydrolysis is carried out at 60 °C, most likely because of the accelerating role of temperature on the hydrolysis process. On the other hand, a further crystalline phase can be appreciated during the time course of the hydrolysis of Sr60 at 60 °C. This phase has been identified as

https://dx.doi.org/10.1021/acs.cgd.0c01569
Cryst. Growth Des. 2021, 21, 1689−1697

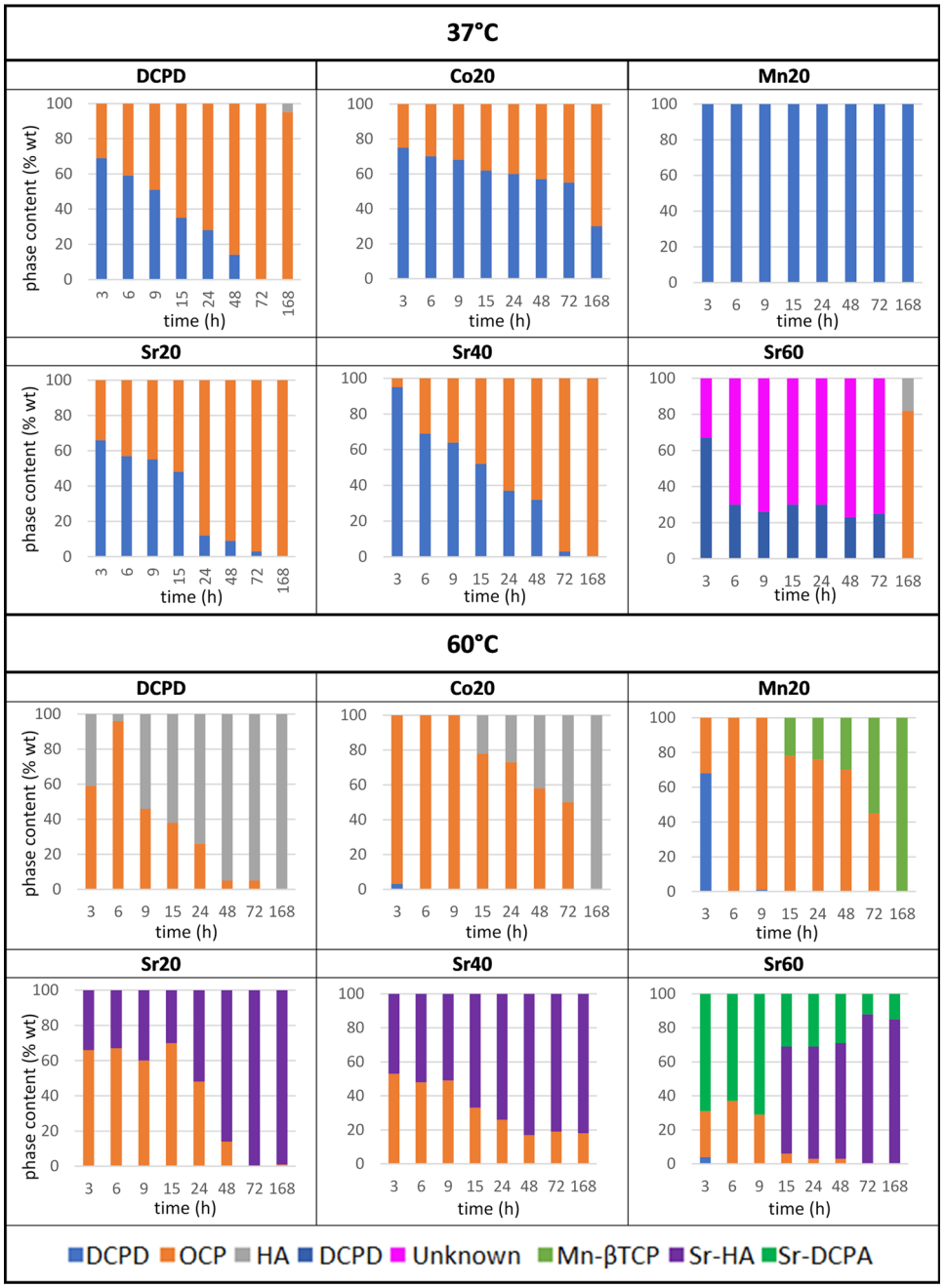

Figure 6. Final crystalline phases obtained after incubation of DCPD, Co20, Mn20, Sr20, Sr40, and Sr60 samples in physiological solution for 1 week at 37 and 60 °C.

DCPA (ICDD PDF 01-070-0359). This DCPA phase, as well as the apatitic phases obtained as products of conversion of the Sr samples at 60 °C, displays enlarged cell parameters in comparison with those of pure DCPA and HA (Table S4), in agreement with a partial substitution of Sr for Ca into their crystalline structures.

CONCLUSIONS

The results of this work highlight the different roles played by different bivalent cations, namely, Sr, Zn, Co, and Mn, in the synthesis and hydrolysis of DCPD. Structural refinements indicate that the ionic radius of substituent cations has a main influence on the extent of possible replacement to calcium. In fact, Sr can be accommodated into the DCPD structure with the largest amount, up to about 38 atom %. Its substitution for calcium induces an enlargement of the unit cell, a shift of the infrared absorption bands, and morphological modification of the typical big platelike crystals of pure DCPD toward aggregates of smaller crystals. Although DCPD can host much lower quantities of Co and Mn, about 2 and 7 atom %, respectively, their influence on the morphology is significantly greater. They not only strongly promote the aggregation but also modify the shape of the crystals. On the other hand, even a small percentage of Zn in solution prevents the synthesis of DCPD as a unique crystalline phase. However, the results of Rietveld refinement of Zn10 suggest a partial replacement of Zn for Ca into the DCPD structure.

https://dx.doi.org/10.1021/acs.cgd.0c01569
Cryst. Growth Des. 2021, 21, 1689−1697

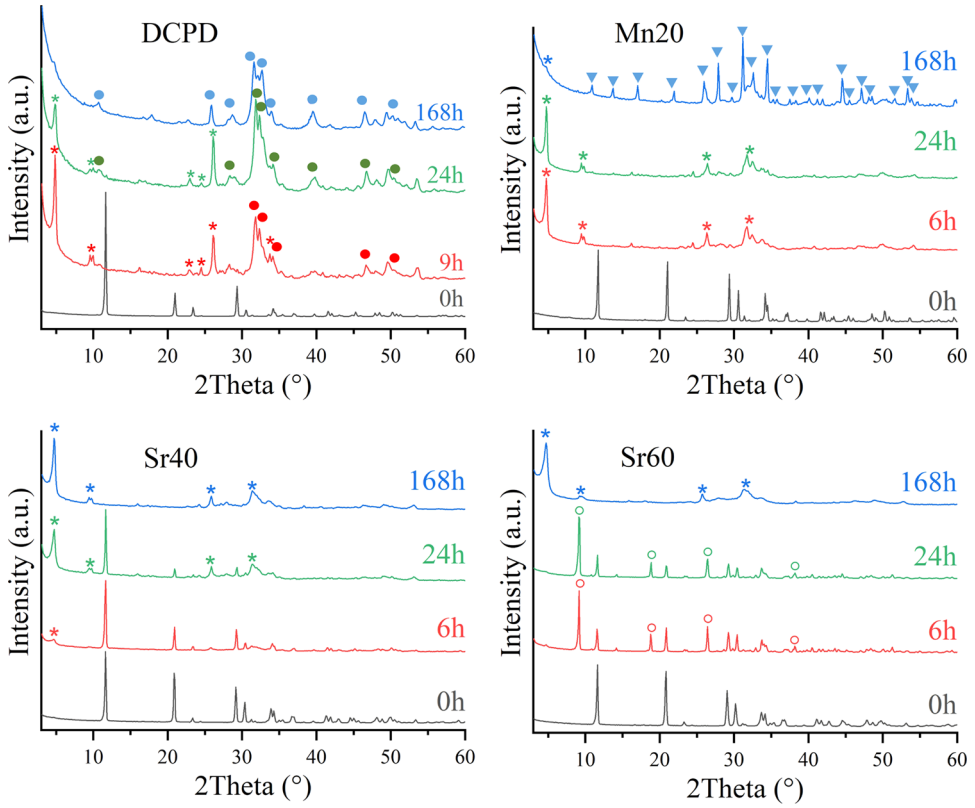

Figure 7. XRD patterns of DCPD and Mn20 samples after incubation at different times in physiological solution at 60 °C and of Sr40 and Sr60 at 37 °C. Symbols: *, OCP (ICDD PDF 00-26-1056); ●, HA (ICDD PDF 00-009-0432); ▼, β-TCP (ICDD PDF 00-009-0169); and ○, unknown crystalline phase.

The most evident effect of the presence of Sr substitution on the hydrolysis process of DCPD is its incorporation into the apatitic phase that forms when the process is carried out at 60 °C. Moreover, hydrolysis of Sr60 leads to the formation of an unknown phase at 37 °C and of Sr-substituted DCPA at 60 °C. Co substitution displays just a slight inhibition of the hydrolysis process of brushite, whereas Mn greatly stabilizes DCPD against the phase transformation in solution at 37 °C. Interestingly, hydrolysis of Mn20 at 60 °C for 1 week triggers its complete transformation into Mn-substituted β-TCP.

A variety of different ions have been found to be associated with the inorganic components of bone, as well as with other calcium phosphates in pathologically calcified tissues. This indicates that the results of this study provide useful information for a better understanding of the mineralization processes of biological tissues. Moreover, since all of the investigated ions are known to display beneficial effects on bone tissues, the materials developed in this work can be considered good candidates as biomaterials for bone substitution/repair.

■ ASSOCIATED CONTENT

Supporting Information

The Supporting Information is available free of charge at https://pubs.acs.org/doi/10.1021/acs.cgd.0c01569.

XRD patterns of all of the solid products obtained in the presence of increasing foreign ion concentration in solution; final plots of Rietveld structural refinements; FTIR spectra of Mn- and Co-substituted samples; and tables that report analytical content (measured by EDAX) of foreign ions in the solid products, yield of reactions, crystalline phases (%) obtained after a hydrolysis reaction of ion-substituted samples, and cell parameters of selected products of hydrolysis and comparison with literature data (PDF)

■ AUTHOR INFORMATION

Corresponding Author

Elisa Boanini − *Department of Chemistry "Giacomo Ciamician", Alma Mater Studiorum University of Bologna, 40126 Bologna, Italy;* orcid.org/0000-0003-3754-0273; Email: elisa.boanini@unibo.it

Authors

Francesca Silingardi − *Department of Chemistry "Giacomo Ciamician", Alma Mater Studiorum University of Bologna, 40126 Bologna, Italy*

Massimo Gazzano − *ISOF-CNR, 40129 Bologna, Italy;* orcid.org/0000-0003-1352-9547

Adriana Bigi − *Department of Chemistry "Giacomo Ciamician", Alma Mater Studiorum University of Bologna, 40126 Bologna, Italy*

Complete contact information is available at: https://pubs.acs.org/10.1021/acs.cgd.0c01569

Author Contributions

The manuscript was written through contributions of all authors. All authors have given approval to the final version of the manuscript.

Notes

The authors declare no competing financial interest.

https://dx.doi.org/10.1021/acs.cgd.0c01569
Cryst. Growth Des. 2021, 21, 1689−1697

■ ACKNOWLEDGMENTS

The authors are grateful to the support of the University of Bologna.

■ REFERENCES

(1) Young, R. A.; Brown, W. E. In *Biological Mineralization and Demineralization*; Nancollas, G. H., Ed.; Springer-Verlag: Berlin, 1982; p 101.
(2) Elliott, J. C. *Structure and Chemistry of the Apatites and Other Calcium Orthophosphates*; Elsevier: Amsterdam, 1994.
(3) Rubini, K.; Boanini, E.; Bigi, A. Role of Aspartic and Polyaspartic Acid on the Synthesis and Hydrolysis of Brushite. *J. Funct. Biomater.* **2019**, *10*, No. 11.
(4) LeGeros, R. Z. Biological and Synthetic Apatites. In *Hydroxyapatite and Related Materials*; Brown, P. W.; Constantz, B., Eds.; CRC Press: Boca Raton, 1979; p 3.
(5) Heughebaert, J. C.; Montel, G. Conversion of Amorphous Tricalcium Phosphate into Apatitic Tricalcium Phosphate. *Calcif. Tissue Int.* **1984**, *34*, 104−108.
(6) Boanini, E.; Gazzano, M.; Rubini, K.; Bigi, A. Collapsed Octacalcium Phosphate Stabilized by Ionic Substitutions. *Cryst. Growth Des.* **2010**, *10*, 3612−3617.
(7) Francis, M. D.; Webb, N. C. Hydroxyapatite Formation from a Hydrated Calcium Monohydrogen Phosphate Precursor. *Calcif. Tissue Int.* **1970**, *6*, 335−342.
(8) Wang, L.; Nancollas, G. H. Calcium Orthophosphates: Crystallization and Dissolution. *Chem. Rev.* **2008**, *108*, 4628−4669.
(9) LeGeros, R. Z. Formation and Transformation of Calcium Phosphates: Relevance to Vascular Calcification. *Z. Kardiol.* **2001**, *90*, 116−124.
(10) Zhang, Z. L.; Chen, X. R.; Bian, S.; Huang, J.; Zhang, T. L.; Wang, K. Identification of Dicalcium Phosphate Dihydrate Deposited during Osteoblast Mineralization in Vitro. *J. Inorg. Biochem.* **2014**, *131*, 109−114.
(11) Dorozhkin, S. V. Calcium Orthophosphates ($CaPO_4$): Occurrence and Properties. *Prog. Biomater.* **2016**, *5*, 9−70.
(12) Gourgas, O.; Khan, K.; Schwertani, A.; Cerruti, M. Differences in Mineral Composition and Morphology between Men and Women in Aortic Valve Calcification. *Acta Biomater.* **2020**, *106*, 342−350.
(13) Zhang, Z. L.; Chen, X. R.; Bian, S.; Huang, J.; Zhang, T. L.; Wang, K. Identification of Dicalcium Phosphate Dihydrate Deposited during Osteoblast Mineralization in Vitro. *J. Inorg. Biochem.* **2014**, *131*, 109−114.
(14) Zhang, J.; Wang, L.; Putnis, C. V. Underlying Role of Brushite in Pathological Mineralization of Hydroxyapatite. *J. Phys. Chem. B* **2019**, *123*, 2874−2881.
(15) Dorozhkin, S. V.; Epple, M. Biological and Medical Significance of Calcium Phosphates. *Angew. Chem., Int. Ed.* **2002**, *41*, 3130−3146.
(16) Tas, A. C.; Bhaduri, S. B. Chemical Processing of $CaHPO_4 \cdot 2H_2O$: Its Conversion to Hydroxyapatite. *J. Am. Ceram. Soc.* **2004**, *87*, 2195−2200.
(17) Shamrai, V. F.; Karpikhin, A. E.; Fedotov, A. Yu.; Sirotinkin, V. P.; Barinov, S. M.; Komlev, V. S. Structural Changes during the Hydrolysis of Dicalcium Phosphate Dihydrate to Octacalcium Phosphate and Hydroxyapatite. *Inorg. Mater.* **2015**, *51*, 355−361.
(18) Zhang, J.; Liu, W.; Schnitzler, V.; Tancret, F.; Bouler, J. M. Calcium Phosphate Cements for Bone Substitution: Chemistry, Handling and Mechanical Properties. *Acta Biomater.* **2014**, *10*, 1035−1049.
(19) O'Neill, R.; McCarthy, H. O.; Montufar, E. B.; Ginebra, M. P.; Wilson, D. I.; Lennon, A.; Dunne, N. Critical Review: Injectability of Calcium Phosphate Pastes and Cements. *Acta Biomater.* **2017**, *50*, 1−19.
(20) Dolci, L. S.; Panzavolta, S.; Torricelli, P.; Albertini, B.; Sicuro, L.; Fini, M.; Bigi, A.; Passerini, N. Modulation of Alendronate Release from a Calcium Phosphate Bone Cement: An *In Vitro* Osteoblast-Osteoclast Co-Culture Study. *Int. J. Pharm.* **2019**, *554*, 245−255.
(21) Bigi, A.; Boanini, E. Functionalized Biomimetic Calcium Phosphates for Bone Tissue Repair. *J. Appl. Biomater. Funct. Mater.* **2017**, *15*, e313−e325.
(22) Bigi, A.; Boanini, E.; Gazzano, M. Ion Substitution in Biological and Synthetic Apatites. In *Biomineralization and Biomaterials: Fundamentals and Applications*; Aparicio, C.; Ginebra, M. P., Eds.; Woodhead Publishing (Elsevier), 2016; pp 235−266.
(23) Shepherd, J. H.; Shepherd, D. V.; Best, S. M. Substituted Hydroxyapatites for Bone Repair. *J. Mater. Sci. Mater. Med.* **2012**, *23*, 2335−2347.
(24) Šupová, M. Substituted Hydroxyapatites for Biomedical Applications: A Review. *Ceram. Int.* **2015**, *41*, 9203−9231.
(25) Arcos, D.; Vallet-Regi, M. Substituted Hydroxyapatite Coatings of Bone Implants. *J. Mater. Chem. B* **2020**, *8*, 1781−1800.
(26) Graziani, G.; Boi, M.; Bianchi, M. A Review on Ionic Substitutions in Hydroxyapatite Thin Films: Towards Complete Biomimetism. *Coatings* **2018**, *8*, No. 269.
(27) Ratnayake, J. T. B.; Mucalo, M.; Dias, G. J. Substituted Hydroxyapatites for Bone Regeneration: A Review of Current Trends. *J. Biomed. Mater. Res., Part B* **2017**, *105*, 1285−1299.
(28) Tite, T.; Popa, A. C.; Balescu, L. M.; Bogdan, I. M.; Pasuk, I.; Ferreira, J. M. F.; Stan, G. E. Cationic Substitutions in Hydroxyapatite: Current Status of the Derived Biofunctional Effects and Their In Vitro Interrogation Methods. *Materials* **2018**, *11*, No. 2081.
(29) Laskus, A.; Kolmas, J. Ionic Substitutions in Non-Apatitic Calcium Phosphates. *Int. J. Mol. Sci.* **2017**, *18*, No. 2542.
(30) Rouzière, S.; Bazin, D.; Daudon, M. In-lab X-ray Fluorescence and Diffraction Techniques for Pathological Calcifications. *C. R. Chim.* **2016**, *19*, 1404−1415.
(31) Alkhraisat, M. H.; Cabrejos-Azama, J.; Rodríguez, C. R.; Jerez, L. B.; Cabarcos, E. L. Magnesium Substitution in Brushite Cements. *Mater. Sci. Eng., C* **2013**, *33*, 475−481.
(32) Schumacher, M.; Gelinsky, M. Strontium Modified Calcium Phosphate Cements − Approaches towards Targeted Stimulation of Bone Turnover. *J. Mater. Chem. B* **2015**, *3*, 4626−4640.
(33) Guerra-López, J. R.; Güida, J. A.; Ramos, M. A.; Punte, G. The Influence of Ni(II) on Brushite Structure Stabilization. *J. Mol. Struct.* **2017**, *1137*, 720−724.
(34) Lee, D.; Kumta, P. N. Chemical Synthesis and Stabilization of Magnesium Substituted Brushite. *Mater. Sci. Eng., C* **2010**, *30*, 934−943.
(35) Sayahi, M.; Santos, J.; El-Feki, H.; Charvillat, C.; Bosc, F.; Karacan, I.; Milthorpe, B.; Drouet, C. Brushite $(Ca,M)HPO_4\ 2H_2O$ Doping with Bioactive Ions (M = Mg^{2+}, Sr^{2+}, Zn^{2+}, Cu^{2+}, and Ag^{+}): a New Path to Functional Biomaterials? *Mater. Today Chem.* **2020**, *16*, No. 100230.
(36) Tian, T.; Han, Y.; Ma, B.; Wu, C.; Chang, J. Novel Co-akermanite ($Ca_2CoSi_2O_7$) Bioceramics with the Activity to Stimulate Osteogenesis and Angiogenesis. *J. Mater. Chem. B* **2015**, *3*, 6773−6782.
(37) Ignjatović, N.; Ajduković, Z.; Rajković, J.; Najman, S.; Mihailović, D.; Uskoković, D. Enhanced Osteogenesis of Nanosized Cobalt-substituted Hydroxyapatite. *J. Bionic Eng.* **2015**, *12*, 604−612.
(38) Mayer, I.; Jacobsohn, O.; Niazov, T.; Werckmann, J.; Iliescu, M.; Richard-Plouet, M.; Burghaus, O.; Reinen, D. Manganese in Precipitated Hydroxyapatites. *Eur. J. Inorg. Chem.* **2003**, *2003*, 1445−1451.
(39) Medvecký, L.; Štulajterova, R.; Parilak, L.; Trpcevska, J.; Durišin, J.; Barinov, S. M. Influence of Manganese on Stability and Particle Growth of Hydroxyapatite in Simulated Body Fluid. *Colloids Surf., A* **2006**, *281*, 221−229.
(40) Sogo, Y.; Ito, A.; Fukasawa, K.; Sakurai, T.; Ichinose, N. Zinc Containing Hydroxyapatite Ceramics to Promote Osteoblastic Cell Activity. *Mater. Sci. Technol.* **2004**, *20*, 1079−1083.
(41) Sutha, S.; Karunakaran, G.; Rajendran, V. Enhancement of Antimicrobial and Long-Term Biostability of the Zinc-Incorporated Hydroxyapatite Coated 316 L Stainless Steel Implant for Biomedical Application. *Ceram. Int.* **2013**, *39*, 5205−5212.

https://dx.doi.org/10.1021/acs.cgd.0c01569
Cryst. Growth Des. 2021, 21, 1689−1697

(42) Yamaguchi, M. Role of Zinc in Bone Formation and Bone Resorption. *J. Trace Elem. Exp. Med.* **1998**, *11*, 119−135.
(43) Peng, S.; Liu, X. S.; Huang, S.; Li, Z.; Pan, H.; Zhen, W.; Luk, K. D. K.; Guo, X. E.; Lu, W. W. The Cross-Talk between Osteoclasts and Osteoblasts in Response to Strontium Treatment: Involvement of Osteoprotegerin. *Bone* **2011**, *49*, 1290−1298.
(44) Dahl, S. G.; Allain, P.; Marie, P. J.; Mauras, Y.; Boivin, G.; Ammann, P.; Christiansen, C.; et al. Incorporation and Distribution of Strontium in Bone. *Bone* **2001**, *28*, 446−453.
(45) Bazin, D.; Dessombz, A.; Nguyen, C.; Ea, H. K.; Lioté, F.; Rehr, J.; Chappard, C.; Rouziere, S.; Thiaudiére, D.; Reguerh, S.; Daudon, M. The Status of Strontium in Biological Apatites: An XANES/EXAFS Investigation. *J. Synchrotron Radiat.* **2014**, *21*, 136−142.
(46) Young, R. A. *The Rietveld Method*; Oxford University Press: Oxford, 1993.
(47) Curry, N. A.; Jones, D. W. Crystal Structure of Brushite, Calcium Hydrogen Orthophosphate Dihydrate: a Neutron-Diffraction Investigation. *J. Chem. Soc. A* **1971**, 3725−3729.
(48) Sikirić, M.; Babić-Ivančić, V.; Milat, O.; Füredi-Milhofer, H.; et al. Factors Influencing Additive Interactions with Calcium Hydrogenphosphate Dihydrate Crystals. *Langmuir* **2000**, *16*, 9261−9266.
(49) Tortet, L.; Gavarri, J. R.; Nihoul, G.; Dianoux, A. J. Study of Protonic Mobility in $CaHPO_4{\cdot}2H_2O$ (Brushite) and $CaHPO_4$ (Monetite) by Infrared Spectroscopy and Neutron Scattering. *J. Solid State Chem.* **1997**, *132*, 6−16.
(50) Hirsch, A.; Azuri, I.; Addadi, L.; Weiner, S.; Yang, K.; Curtarolo, S.; Kronik, L. Infrared Absorption Spectrum of Brushite from First Principles. *Chem. Mater.* **2014**, *26*, 2934−2942.
(51) Fowler, B. O. Infrared Studies of Apatites. II. Preparation of Normal and Isotopically Substituted Calcium, Strontium, and Barium Hydroxyapatites and Spectra-Structure-Composition Correlations. *Inorg. Chem.* **1974**, *13*, 207−214.
(52) Fulmer, M. T.; Brown, P. W. Hydrolysis of Dicalcium Phosphate Dihydrate to Hydroxyapatite. *J. Mater. Sci. Mater. Med.* **1998**, *9*, 197−202.
(53) Mayer, I.; Cuisinier, F. J. G.; Popov, I.; Schleich, Y.; Gdalya, S.; Burghaus, O.; Reinen, D. Phase Relations Between β-Tricalcium Phosphate and Hydroxyapatite with Manganese(II): Structural and Spectroscopic Properties. *Eur. J. Inorg. Chem.* **2006**, *2006*, 1460−1465.
(54) Rau, J. V.; Fadeeva, I. V.; Fomin, A. S.; Barbaro, K.; Galvano, E.; Ryzhov, A. P.; Murzakhanov, F.; Gafurov, M.; Orlinskii, S.; Antoniac, I.; Uskoković, V. Sic Parvis Magna: Manganese-Substituted Tricalcium Phosphate and Its Biophysical Properties. *ACS Biomater. Sci. Eng.* **2019**, *5*, 6632−6644.
(55) Tas, A. C. Transformation of Brushite ($CaHPO_4{\cdot}2H_2O$) to Whitlockite($Ca_9Mg(HPO_4)(PO_4)_6$) or Other CaPs in Physiologically Relevant Solutions. *J. Am. Ceram. Soc.* **2016**, *99*, 1200−1206.

https://dx.doi.org/10.1021/acs.cgd.0c01569
Cryst. Growth Des. 2021, 21, 1689−1697